Slope stability estimation using a Danger Level approach for monitoring landslide prone areas

Siti Nurbaidzuri Reli[1], Izham Mohamad Yusoff[1], Muhamad Uznir Ujang[2]

[1]Geography Section, School of Distance Education, Universiti Sains Malaysia, 11800 USM Penang, Malaysia.
[2]Department of Geoinformation, Faculty of Build Environment and Survey, Universiti Teknologi Malaysia, 81310 Skudai, Johor Darul Takzim, Malaysia.

Correspondence: Izham Mohamad Yusoff (email: izham@usm.my)

Received: 29 May 2021; Accepted: 30 August 2021; Published: 30 November 2021

Abstract

Slope stability evaluation is an essential element in assessing landslide hazards and ensuring the safe design of structures and infrastructure. There has been increased awareness of the need to give greater attention to these phenomena. However, there is no general rule for classifying safety factors of the slope. The factor of safety (FOS) is used globally to determine slope stability by identifying shear strength and shear stress. However, the FOS cannot become the only assessment to evaluate slope stability. This research focuses more on the infiltration of soil-water that reduces the strength of slopes based on the danger level (DL). DL is divided into four categories: low, moderate, high, and very high. To estimate slope stability, four main locations are set on the slope: P1 (highest point), P2, P3 and P4 (lowest point). The DL value is determined using FOS, a rainfall threshold, soil-water infiltration, and soil classification. The DL value for P1 is 0.567 (moderate risk), while the DL values for P2, P3, and P4 are 0.116, 0.073, and 0.095 (very high risk), respectively, indicating that this slope is hazardous. Determining hazardous slope points will be easier, as DL has classified specific slope locations with exact risk values.

Keywords: Danger Level (DL), Factor of Safety (FOS), landslide, rainfall, slope stability, soil-water infiltration

Introduction

Slope instability is one of the major challenges faced by practitioners and researchers in monitoring natural and man-made slopes. Slope instability is generally triggered by prolonged rainfall, downpour, rise of groundwater, monsoon, flood, mining and construction. Another source of frequent landslides is long-term changes over the Earth's elevation surface (Gariano and Guzzetti, 2016; Haque et al., 2019). Slope changes due to external forces also lead to slope failure due to a loss of shear strength, leading to a landslide. Landslides are the most prevalent geomorphological processes in mountainous regions and can catastrophically damage local communities (Tian et al., 2019; Guo et al., 2020). External causes that influence slope stability

include the alteration that occurs in slope geometry. This includes the removal of lateral support through undercutting, loading, or unloading and erosion or artificial unearthing (Hansen, 1984; Cruden and Varnes, 1996).

The importance of slope stability contributes to the development of many alternative methods for assessing the safety of slopes. However, there is no general rule on the classification of safety factors (Borges et al., 2015). The basic approach is to determine a factor of safety (FOS) against failure for a given slope (Khalaj et al., 2020; Fabrizio de Luiz et al., 2020) and this method differs in simplification and accuracy (Pourkhosravani and Kalantari, 2011). Van Westen and Terlien (1996) categorized the FOS into three classes: unstable slope (below 1), moderate stability (between 1 and 1.50) and stable slope (above 1.50). On the other hand, Pradhan and Siddique (2020) classified a FOS between 1 and 1.30 as moderate stability and above 1.30 as a stable slope. Since there are different opinions regarding moderate and stable slopes, this research only defines slopes as stable or unstable based on FOS values that are more or less than 1, respectively. The main criteria required to measure the danger level (DL) of the slope in this research are rainfall, soil-water infiltration, FOS and soil characteristics as defined by OSHA.

Studies have shown that 0.53% of deaths and 14% of economic losses are due to rainfall-induced landslides, which occur almost annually in most mountainous regions (Hidalgo and Vega, 2014). This statement is consistent with Liu and Li (2015) and Ivanov et al. (2020). This research emphasizes the importance of infiltrating rainfall because this contributes to slope instability and triggers landslides by weakening the bonds between soil particles. Geological hazards such as infiltration-related landslides affect many people every year through increasing costs of restoration, destruction of property and loss of life.

To monitor landslides in large areas, research was conducted in which hydrological behaviour was combined with the evaluation of slope stability (Casagli et al., 2005; Tsai et al., 2008). Geographic information systems (GISs) have evolved and have become more relevant for landslide risk management purposes (Kim et al., 2014; Gutiérrez-Martín, 2020). Although most studies have acknowledged the essential importance of changes in water movement and pressure transfer through unsaturated soils, they have ignored the effect of the hydrological behaviour of variable stress saturation on effective stress and soil strength. The amount of water in the hills and water table vary as the water enters the slope. As a result, the effective change in soil matrix suction, suction stress and unit total weight significantly reduce the stability throughout the slope. Many studies have evaluated these results by combining hydrological process models and slope stability assessments (Borja and White, 2010; Vahedifard et al., 2016). However, effective early warning of landslides remains a challenge, requiring the acquisition of additional information and data (Alexandra et al., 2019). As a result, this study develops a danger level (DL) approach for estimating slope stability through the integration of slope and environmental conditions.

Methods and study area

The final measure of landslide prediction can be examined by using DL values of the slope based on varying precipitation intensity, soil-water infiltration, FOS and soil classification. Analyses attempted to explain the slope failure triggering mechanisms and the variables that can potentially initiate a slope movement leading to a landslide. In addition, this research hoped to mitigate such a movement by decelerating or stopping it by using mitigating countermeasures. The study area is located on the Gerik-Jeli Highway in Perak with coordinates 101°35'13.868"E and 5°36'7.948"N (Figure 1).

The danger level (DL) approach was developed to estimate slope risk. Mathematical

computing was built in the open-source software, namely, Processing 3, resulting in the DL slope risk classification. The main components used to estimate the DL of the slope are illustrated in Figure 2.

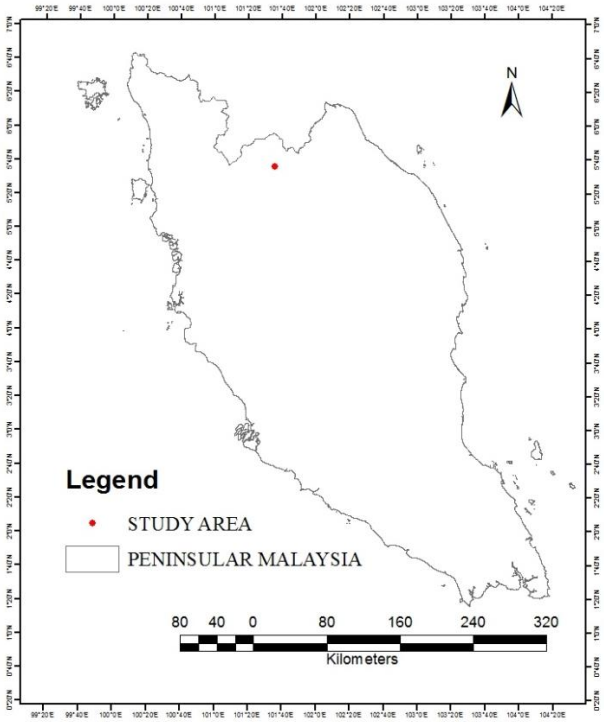

Figure 1: The study area is located on the Gerik-Jeli highway.

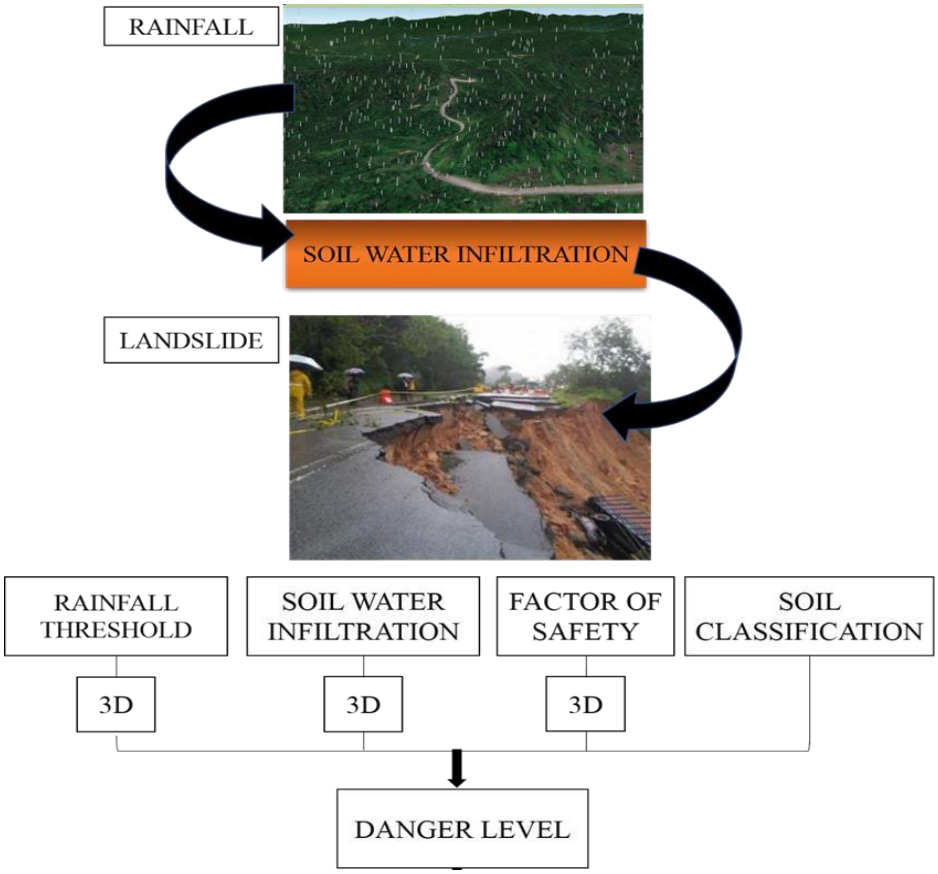

Figure 2. The important components used to estimate the danger level (DL) of the slope.

Rainfall threshold

Prolonged rainfall can have a major effect on the infiltration of soil-water by reducing its soil resistance. An antecedent precipitation analysis was employed in this study to estimate the rainfall threshold formulated by Glade et al. (2000) and used by Zhao et al. (2019) and Chikalamo et al. (2020). Rainfall data from six landslides were collected to determine the rainfall threshold that could trigger a landslide. The antecedent daily rainfall model was used as a proxy of the soil moisture index to assess the rainfall antecedent threshold. The index indicated the moisture of the soil in the days before the real landslide occurred. Before the rainfall threshold can be determined, the weight-effective antecedent rainfall (AR_x) needs to be calculated. A similar method was used in Zêzere et al. (2005) and Glade et al. (2000), and the equation for AR_x is:

$$AR_x = KP_1 + K^2P_2 + ..+K^nP_n \quad (1)$$

Where,
P_1 : Daily rain (before dayX)
P_n : Daily rain (nth day before dayX)

Soil water infiltration

Some data were not available but are essential to measure the mechanism of soil infiltration. Thus, the hydrological and soil science equation was used mainly to generate the relevant data. Permeability was one of the necessary parameters for the infiltration component. The permeability of the soil is determined using the falling head permeability test (2).

$$K = \left[\frac{2.3\ a.L}{A.\Delta t}\right].Log\left(\frac{h\_U}{h\_L}\right) \quad (2)$$

a : cross-section (standpipe)
h_U : upper and lower water level (standpipe)
h_L : lower water level (standpipe)
L : soil column high (sample)
A : cross-section (sample)
Δt : water column to flow time

The slope is composed of seven soil layers containing six different soil types. Each type of soil requires a value of hydraulic conductivity K_{sat} (cm/hour). By using the available moisture content and specific gravity data, it is necessary to determine three inaccessible but important parameters, which include porosity (η), effective porosity (θ_c) and wetting front (ψ_f). The void ratio is required to determine the effective porosity (θ_c) with Equation (3):

$$e = moisture\ content \times g \quad (3)$$

e: void ratio
g: gravity

With (3), the soil porosity is determined by the following equation:

$$e = \frac{n}{n-1} \quad (4)$$

n: porosity

Then, (4) is used to calculate moisture content θ_r :

$$\theta_r = n - \theta_e \quad (5)$$

θ_r : moisture content (residual)
θ_e: effective porosity of soil

Rawls et al. (1982) introduced the hydraulic conductivity $K_{sat,}$ and based on previous studies, an elevated water content accommodated by dry soil represents efficient porosity. Hydraulic conductivity (K_{sat}) and effective porosity (θ_c) values cannot be derived from previous studies and research due to the diverse soil types in the study area. It is important information used in the Green and Ampt method, as well as the multilayer Green and Ampt method. Effective saturation (S_e) can be calculated based on Equation (6):

$$S_e = \frac{\theta_i - \theta_r}{n - \theta_r} \quad (6)$$

θ_i: initial moisture content

According to Chow et al., (1988), the wetting front ($\Delta\theta$) can be acquired with Equation (7):

$$\Delta\theta = \theta_c\ (1 - S_e) \quad (7)$$

S_e: Effective saturation
θ_c: Effective porosity

The Green and Ampt method introduced by Green and Ampt (1911) provides a computation method to determine the infiltration rate and cumulative infiltration for various soil classes. The first layer of the soil was calculated by using the Green and Ampt method. GSSHA (gridded surface/subsurface hydrologic analysis) introduced by Downer et al. (2005) adapted the multilayer Green and Ampt model. GSSHA uses this equation to determine the saturated hydraulic conductivity (K^n) for three soil horizons. For this research, to comply with the suitability of the analysis, the multilayer Green and Ampt model was expanded from the original version. The slope is composed of seven soil layers divided into four major points (P1, P2, P3 and P4), requiring repeated measurements resulting in 28 infiltration values (Figure 3).

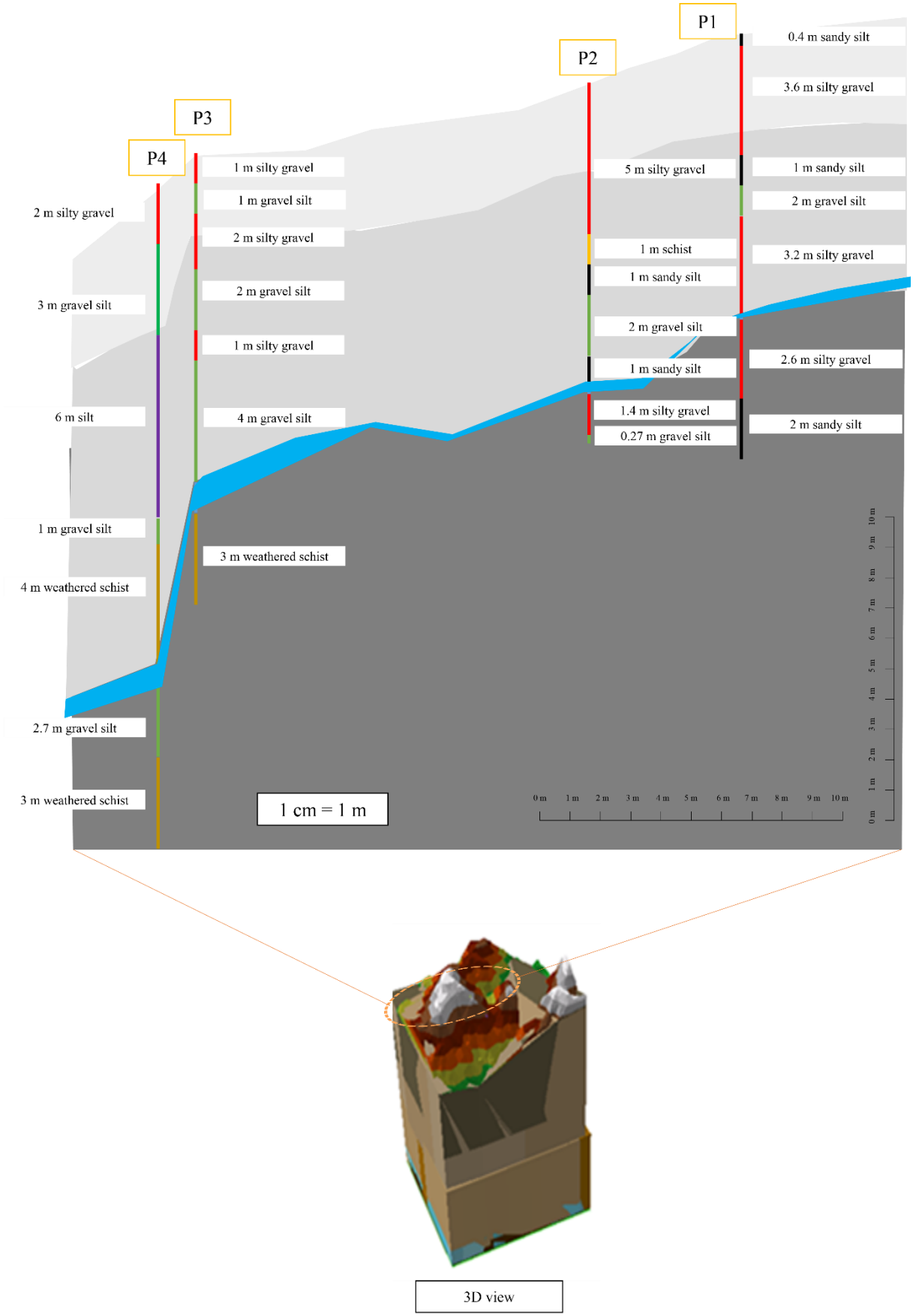

Figure 3. The four main monitored locations on slope surface.

For the first layer of soil, K_{sat} is based on recorded values according to soil types. The multilayer Green and Ampt model equation starts to be used in the second layer of soil. The equation of K_{sat} for the 2nd layer to 7th layer is shown in Equations 8 to 13:

$$K^n = \frac{\left(L_1 + \frac{F^n - L_1\,\Delta\theta_1}{\Delta\theta_2}\right)}{\left(\frac{L_1}{K_1} + \left(\frac{\frac{F^n - L_1\,\Delta\theta_1}{\Delta\theta_2}}{K_2}\right)\right)} \quad (8)$$

$$K^n = \frac{\left(L_1 + L_2 + \frac{F^n - (L_1\,\Delta\theta_1 + L_2\,\Delta\theta_2)}{\Delta\theta_3}\right)}{\left(\frac{L_1}{K_1} + \frac{L_2}{K_2} + \left(\frac{\frac{F^n - (L_1\,\Delta\theta_1 + L_2\,\Delta\theta_2)}{\Delta\theta_3}}{K_3}\right)\right)} \quad (9)$$

$$K^n = \frac{\left(L_1 + L_2 + L_3 + \frac{F^n - (L_1\,\Delta\theta_1 + L_2\,\Delta\theta_2 + L_3\,\Delta\theta_3)}{\Delta\theta_4}\right)}{\left(\frac{L_1}{K_1} + \frac{L_2}{K_2} + \frac{L_3}{K_3} + \left(\frac{\frac{F^n - (L_1\,\Delta\theta_1 + L_2\,\Delta\theta_2 + L_3\,\Delta\theta_3)}{\Delta\theta_4}}{K_4}\right)\right)} \quad (10)$$

$$K^n = \frac{\left(L_1 + \cdots + L_4 + \frac{F^n - (L_1\,\Delta\theta_1 + \cdots + L_4\,\Delta\theta_4)}{\Delta\theta_5}\right)}{\left(\frac{L_1}{K_1} + \cdots + \frac{L_4}{K_4} + \left(\frac{\frac{F^n - (L_1\,\Delta\theta_1 + \cdots + L_4\,\Delta\theta_4)}{\Delta\theta_5}}{K_5}\right)\right)} \quad (11)$$

$$K^n = \frac{\left(L_1 + \cdots + L_5 + \frac{F^n - (L_1\,\Delta\theta_1 + \cdots + L_5\Delta\theta_5)}{\Delta\theta_6}\right)}{\left(\frac{L_1}{K_1} + \cdots + \frac{L_5}{K_5} + \left(\frac{\frac{F^n - (L_1\,\Delta\theta_1 + \cdots + L_5\Delta\theta_5)}{\Delta\theta_6}}{K_6}\right)\right)} \quad (12)$$

$$K^n = \frac{\left(L_1 + \cdots + L_6 + \frac{F^n - (L_1\,\Delta\theta_1 + \cdots + L_6\Delta\theta_6)}{\Delta\theta_7}\right)}{\left(\frac{L_1}{K_1} + \cdots + \frac{L_6}{K_6} + \left(\frac{\frac{F^n - (L_1\,\Delta\theta_1 + \cdots + L_6\Delta\theta_6)}{\Delta\theta_7}}{K_7}\right)\right)} \quad (13)$$

Where:

F^n	:	Soil water Cumulative Infiltration (n time)
K	:	Saturated hydraulic conductivity of the soil
L	:	Thickness (soil horizon)
1-7	:	soil layer 1 - 7

Cumulative infiltration F(t) can be calculated based on the outcome of K_{sat}. The first layer used the accumulated value for infiltration. The following layers apply cumulative infiltration F(t) based on Equation (14):

$$F(t) = F^n + K^n(\Delta t) + \psi_f\,\Delta\theta ln\left(\frac{F(t) + \psi_f\Delta\theta}{F^n + \psi_f\Delta\theta}\right) \quad (14)$$

Δt	:	n - θ_c
K^n	:	Saturated Hydraulic Conductivity
ψ_f	:	Wetting front

The solution needs to calculate the infiltration rate f(t) of each soil layer. The infiltration duration is measured in cm per hour using Equation (15):

$$f(t) = K^n \left(\frac{\psi_f \, \Delta\theta}{F(t)} + 1\right) \quad (15)$$

F(t) : Cumulative infiltration

Slope stability based on Factor of Safety (FOS)

In soil engineering, the infinite slope model is used to evaluate the slope stability affected by soil-water infiltration (Phoon, 2008). Biondi et al. (2000) introduced the equation of infinite slope that is widely used in slope stability studies (Travis et al., 2009; Griffiths et al., 2011; Kang et al., 2020). The infinite stability method assumes homogeneous properties of the soil where fractures occur. In this study, the FOS Equation (16) was applied at four locations within a single slope with varying soil types: soil specific gravity, porosity, angle of inclination, effective cohesion, pore water pressure, angle of effective internal friction and thickness.

$$FS = \left(\frac{(h\gamma cos^2\,\theta - \mu)\tan\varphi' + c\prime}{h\gamma \sin\theta \cos\theta}\right) \quad (16)$$

The saturated soil unit weight (γ') calculated using Equation (17):

$$\gamma' = \gamma_w \left(\frac{G_s + e}{1 + e}\right) \quad (17)$$

Resisting force normal (S_{normal}) (18) of the slope is required to determine resisting force (S) (19).

$$S_{normal} = h \times \gamma' \times \theta \quad (18)$$

Pore pressure (μ) acts as a counter to the normal pressure, which weakens the downward force, while cohesion (c) represents the tension of the water surface. Soil thickness (h) is the distance from the soil surface to the bedrock. Since this study focuses on soil-water infiltration, Equation (19) is most relevant:

$$S = S_{normal} - \mu \text{ x } \tan\varphi + c \quad (19)$$

The driving force (τ) is calculated using Equation (20).

$$\tau = h \times \gamma' \times sin\ sin\ \theta\ \ cos\ cos\ \theta \quad (20)$$

Where:

γ' : Unit specific weight (kg/m^3) of soil
γ_w : Unit specific weight (kg/m^3) of water
G_s : The specific gravity of soil (N/kg)
e : Void ratio
c' : Effective cohesion (N/m^3)
μ : Pore pressure (N/m^2)
h : Thickness (m)

θ : Slope angle
φ' : Effective coefficient of internal friction (degree)

The final calculation of the FOS is as follows:

$$F = \frac{S}{\tau} \tag{21}$$

If F < 1 (unstable slope)
If F > 1 (stable slope)

Soil classification

According to excavation resilience, OSHA classified soil into types A, B, and C, ranging from the most stable (solid rock) to the least stable (type C). This research uses this classification to evaluate soil-based slope strength. The excavation process alters the slope's original shape and condition. The slope of the study area was explored where the original slope form was altered due to excavation. The undisturbed slope rarely causes slope failure. The OSHA classification is used as one of the criteria for determining the slope stability depending on the soil type.

Danger Level (DL) approach to define slope strength based on danger score

A combination of the important parameters resulted in DL values, and the findings provided a new approach to predict the possibility of landslides. The main parameters are FOS, rainfall, soil-water infiltration, and OSHA soil classification. To coordinate the decision by implementing a structured approach, a basic analytical hierarchy method (AHP) was used to assign parameters based on priority (Figure 4).

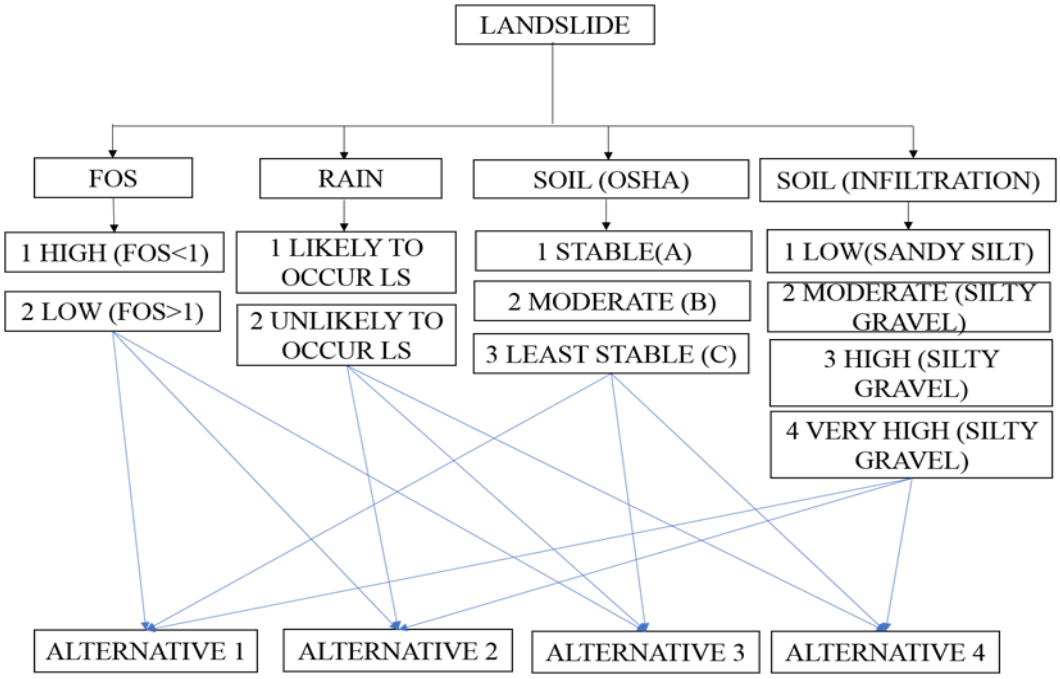

Figure 4. Criteria and alternative in the Analytical Hierarchy Process (AHP).

For each element, the percentage was divided according to preference. This research offers a way to plan and distribute percentages based on rankings to prioritize each element. The total value is 100, which is then converted to 1. The risk score ranges from zero to one, where a value close to zero is dangerous because it has the highest risk level factor. On the other hand, a DL value close to 1 is regarded as having a low risk. The newly developed DL for estimating slope stability is based on the following Equation (22):

$$DL: FDS + ODS + RDS + SDS \quad (22)$$

DL	Very high	0 - 0.25
DL	High	0.26 - 0.50
DL	Moderate	0.51 - 0.75
DL	Low	0.76 - 1

Where:

F DS	:	FOS danger score
O DS	:	OSHA danger score
R DS	:	Rainfall danger score
S DS	:	Soil danger score

Results and discussion

The pattern of precipitation-induced rainfall was determined based on six landslides with hourly rainfall data, and a similar method was used in Zhao et al. (2019) and Chikalamo et al. (2020). Previous precipitation analysis was used to estimate soil moisture before a hurricane (Hughes, 1998). The daily rainfall intensity data were gathered 15 days before the landslide (Table 1). The reduction coefficient (α_t) represents ½ of (α_{t-1}).

Table 1. Antecedent working rainfall (R_{WA})

Rainfall Intensity						Deduction Coefficient (α_t)	Before Event Day (P)
13.12.07	**11.09.13**	**13.09.13**	**14.09.13**	**23.12.14**	**17.12.14**		
8.5	1.3	1.1	1.2	10	12.8	0.5	1
1.5	35.3	1.3	1.1	14.8	28	0.25	2
0	63.7	23.5	1.3	5.3	6.3	0.125	3
0	19.3	63.7	23.5	3	1	0.0625	4
0	18.4	19.3	63.7	1.8	0	0.03125	5
0	46.2	18.4	19.3	1.8	0	0.01563	6
1	45.3	46.2	18.4	12.8	0	0.00781	7
15.5	7.7	45.3	46.2	28	0	0.00391	8
0	6.2	7.7	45.3	6.3	0	0.00195	9
1.5	0	6.2	7.7	1	1.5	0.00098	10
8.5	4.7	0.0	6.2	0	7	0.00049	11
0.5	0	4.7	0.0	0	0.8	0.00024	12
0	0	0.0	4.7	0	0	0.00012	13
5	0	0.0	0.0	0	0.3	0.00006	14
5	0	0.0	0	0	2.5	0.00003	15

The accumulated antecedent working rainfall (Table 2) was obtained by multiplying the rainfall rate by the reduction factor for P_1. The cumulative antecedent working rate increased from Day 1 (P_1) to Day 15 (P_{15}). A high frequency of landslides was due to the high value of rainfall intensity, which corresponded to three consecutive rain storms a few days before the landslide (P_1, P_2 and P_3). The other four landslides had high rainfall from eight to four days before the landslide, resulting in a reduction in previous cumulative rainfall. However, the value decreased as it got closer to the days of the event. These results suggest that the landslide was generally triggered by light rain on the day of the landslide, preceded by 15 days of continuous rain.

Table2. Cumulative Antecedent Working Rainfall for six landslide events.

Cumulative Antecedent Working Rainfall for 15 Days						Days Before Event (P)
13.12.2007	**11.09.2013**	**13.09.2013**	**14.09.2013**	**23.12.2014**	**17.12.2014**	
4.25000	0.65000	0.55000	0.60000	5.00000	6.40000	1
4.62500	9.47500	0.87500	0.87500	8.70000	13.40000	2
4.62500	17.43750	3.81250	1.03750	9.36250	14.18750	3
4.62500	18.06475	5.88275	1.80125	9.46000	14.22000	4
4.62500	18.63975	6.48588	3.79188	9.51625	14.22000	5
4.62500	19.36186	6.77347	4.09353	9.54438	14.22000	6
4.63281	19.71565	7.13429	4.23724	9.64435	14.22000	7
4.69342	19.74576	7.31141	4.41788	9.75383	14.22000	8
4.69343	19.75785	7.32642	4.50622	9.76612	14.22000	9
4.69489	19.75785	7.33250	4.51377	9.76710	14.22147	10
4.69905	19.76015	7.33250	4.51680	9.76710	14.22490	11
4.69917	19.76015	7.33363	4.51680	9.76710	14.22509	12
4.69917	19.76015	7.33363	4.51736	9.76710	14.22509	13
4.69947	19.76015	7.33363	4.51736	9.76710	14.22511	14
4.69962	19.76015	7.33363	4.51736	9.76710	14.22519	15

To prepare a landslide threshold graph, data from 3 days (P_3) and 15 days (P_{15}) were required prior to this event, as both short and long rainfalls can accelerate landslides. These results used to indicate rainfall conditions affects landslides where the threshold acts as a level of volume. The rainfall pattern is defined as $P_3 = 6.075 - 0.309\ P_{15}$ (Table 3). The rainfall threshold (CT) prepares a graft prediction that shows the pattern of rain that is likely or unlikely to cause landslides. The five hazardous hazards are above the linear line, indicating the possibility of landslides. Only one of the landslide events positioned below the linear line suggests that landslides are unlikely to occur. The outcomes indicated that landslides are significantly influenced by rainfall in Malaysia.

Table 3. Rainfall threshold (CT).

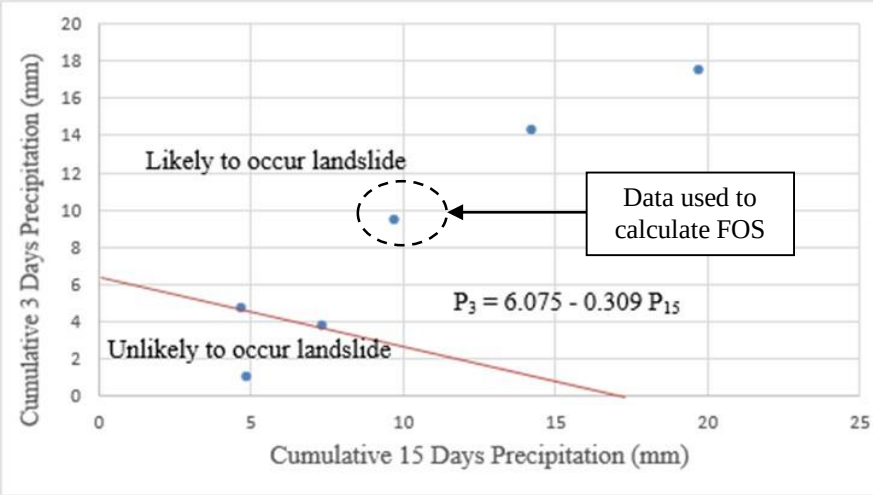

The rainfall intensity and cumulative rainfall used to calculate FOS were the data on 23rd December 2014, which are highlighted in Table 1 and Table 2. These data were chosen because this rainfall led to 20 landslides along the East-West Gerik-Jeli Highway, including the slope in the study area.

The extended multilayer Green and Ampt method was used to determine the next layer of infiltration f(t), cumulative infiltration (F)t and hydraulic conductivity (K_n). The process was performed for every point of the slope (P1, P2, P3, and P4) that had seven layers of soil. Before infiltration rate f(t) and cumulative infiltration F(t) could be determined, every parameter necessary for the calculation is listed in Table 4.

Table 4. Cumulative infiltration and hydraulic conductivity of soil using the multilayer Green and Ampt method.

SOIL ID	TYPE	η	$\Delta\theta$	ψ	K_{sat}	F_n	K_n
P1L1	Sandy silt	0.43	0.1804	44.3	0.3	2.22	
P1L2	Silty gravel	0.35	0.1946	64.5	0.4	3.03	0.194
P1L3	Sandy silt	0.43	0.1304	41	0.3	3.33	0.183
P1L4	Gravel silt	0.39	0.1592	53.9	0.4	5.21	0.952
P1L5	Silty gravel	0.35	0.2146	62.2	0.4	5.94	0.305
P1L6	Silty gravel	0.35	0.2546	62.4	0.4	6.68	0.343
P1L7	Sandy silt	0.43	0.3204	32.9	0.3	7.89	0.802
P2L1	Silty gravel	0.35	0.1446	54.9	0.4	2.62	
P2L2	Schist	0.39	0.3921	69.6	0.9	4.04	0.308
P2L3	Sandy silt	0.43	0.2904	17.8	0.3	7.22	2.736
P2L4	Gravel silt	0.39	0.1492	45.8	0.4	7.7	0.408
P2L5	Sandy silt	0.43	0.2304	40.4	0.3	8.75	0.8
P2L6	Silty gravel	0.35	0.1246	51	0.4	9.15	0.427
P2L7	Gravel silt	0.39	0.1192	47.7	0.4	9.59	0.456
P3L1	Silty gravel	0.35	0.1546	63.3	1.5	5.98	
P3L2	Gravel silt	0.39	0.1592	36.9	0.4	6.54	0.505
P3L3	Silty gravel	0.35	0.0746	47.1	1.5	7.76	1.442

P3L4	Gravel silt	0.39	0.0992	43.1	0.4	7.78	0.023
P3L5	Silty gravel	0.35	0.1546	39	1.5	8.13	0.327
P3L6	Gravel silt	0.39	0.2492	50.7	0.4	10.3	1.485
P3L7	Weathered schist	0.56	0.56	37.4	0.8	11.2	0.496
P4L1	Silty gravel	0.35	0.1846	49.6	0.4	2.8	
P4L2	Gravel silt	0.39	0.1492	49.6	0.4	3.75	0.49
P4L3	Silt	0.3	0.1418	77.6	1.5	3.87	0.057
P4L4	Gravel silt	0.39	0.1492	57.5	0.4	3.89	0.008
P4L5	Weathered schist	0.56	0.56	37.4	0.8	5.96	0.593
P4L6	Gravel silt	0.39	0.0092	59.5	0.4	6.23	0.404
P4L7	Weathered schist	0.56	0.56	37.4	0.8	6.9	0.537

The results of the infiltration rate f(t) and cumulative infiltration F(t) of the slope are shown in Table 5.

Table 5: Infiltration rate and cumulative infiltration of Layer 1 to Layer 7.

		POINT 1		POINT 2		POINT 3		POINT 4	
	Hour	F(t)	f(t)	F(t)	f(t)	F(t)	f(t)	F(t)	f(t)
L1	1	2.2188	1.33515	2.62312	1.61275	5.98062	4.05016	2.80457	1.70788
	12	3.87802	0.88794	4.5889	1.09351	10.5088	2.96716	4.90433	1.1482
	24	5.68808	0.69763	6.7334	0.87284	15.4486	2.50978	7.19496	0.9102
L2	1	3.02643	0.99816	4.04191	2.38475	6.53541	0.95883	3.74843	1.45699
	12	3.77615	0.83846	5.2748	1.89924	7.02472	0.9272	4.57528	1.28215
	24	4.59403	0.7237	6.61977	1.57585	7.55851	0.89736	5.4773	1.15162
L3	1	3.32651	0.47628	7.22341	4.69938	7.75854	2.09415	3.87335	0.21888
	12	3.60018	0.45396	9.99586	4.15495	8.83663	2.01455	3.98361	0.2144
	24	3.89872	0.43318	13.0203	3.82545	10.0127	1.94726	4.10389	0.20979
L4	1	5.20978	2.51875	7.69863	0.77107	7.77961	0.03498	3.88875	0.02552
	12	6.91181	2.13292	8.13241	0.75172	7.79886	0.03495	3.90281	0.02546
	24	8.76857	1.88283	8.60561	0.73283	7.81986	0.03491	3.91816	0.02539
L5	1	5.93551	0.99173	8.74532	1.65116	8.12703	0.56876	5.96227	2.67725
	12	6.5966	0.92286	9.6996	1.5674	8.44426	0.55966	7.83364	2.17937
	24	7.31779	0.86192	10.7406	1.493	8.79034	0.55049	9.87514	1.85145
L6	1	6.68076	1.16028	9.14815	0.72413	10.3322	3.30151	6.22747	0.43932
	12	7.35987	1.08491	9.51602	0.71266	12.3378	3.00619	6.46974	0.43799
	24	8.10072	1.0171	9.91733	0.70111	14.5258	2.77702	6.73403	0.43665
L7	1	7.89489	1.87141	9.59173	0.72671	11.2254	1.42249	6.90074	2.16684
	12	9.00071	1.74002	9.99677	0.71575	12.0401	1.35981	7.51487	2.03363
	24	10.2071	1.62916	10.4386	0.70476	12.9288	1.30045	8.18483	1.91112

This method can provide a fixed rate of infiltration, which depends on the soil type that gives an accurate reading of the water flow in the soil. Deep soils have a slow infiltration rate and eventually reach a steady state. In terms of sediment yield, fires can significantly increase surface erosion by removing protective vegetation and, in some cases, by creating a hydrophobic surface that inhibits infiltration and promotes overland flow (Stine, 2013). The primary cause of landslides is due to gravity because it reduces the strength of the slope materials. In some situations, a landslide forms gradually as time passes, but the situation worsens with elements such as earthquakes or rainfall. Infiltrated soil-water can modify the

slope's strength, making it unstable. Water seeps into the soil material, making it heavier and succumbing to the force of gravity. Excess water in the soil caused by heavy rains in Malaysia usually causes slope instability, requiring immediate intervention. Table 6 shows the data needed to calculate the stability of slopes based on the FOS. For FOS, only the data for P1, P2, P3 and P4 on the slope surface were used. The data in Tables 4 and 5 were used to examine the rate of water movement through every soil layer. This is significant because the ease of soil-water movement beneath the soil varies from one type of soil to another, affecting the slope surface stability. Since every layer consists of different types of soil, the computation of K_n, F(t) and f(t) for all layers is essential.

Table 6. Information on the slope.

	P 1	P 2	P 3	P 4
Thickness (m)	10.4	11	12	16.3
Density (kg/m^3)	2028.372	2121.48	2031.6	2251.954
Gravity (N/kg)	2.8042	2.7365	2.6875	2.7977
Slope Angle (°)	37.651	31.269	39.04	37.298
Cohesion (N/m^3)	11000	10000	10000	10000
Pore pressure (N/m^3)	32300	23500	26900	45700

The FOS value is required to indicate the section of the slope between P1 and P4 with the lowest to the strongest strength. The lowest FOS value of the slope shows the exact location that has a high possibility of initiating landslides that require close surveillance. P2, P3, and P4 are lower than one, indicating that the slope was not steady. However, the stable P1 at the very top of the slope is affected by the unstable lower structure. The FOS value from P1 to P4 is shown in Table 7.

Table 7. FOS for every point on the slope.

FACTOR OF SAFETY P1	1.4474187
FACTOR OF SAFETY P2	0.65168417
FACTOR OF SAFETY P3	0.8579746
FACTOR OF SAFETY P4	0.4113201

P1 is the only point on the slope with sandy silt soil. The remaining points consist of a similar soil type, which is silty gravel. Despite similar soil types, pore water pressure changed from P2 to P4. The highest pore water pressure is at the bottom of the slope (P4). The increase in pore water pressure from P2 to P4 is due to the soil position descending from the slope. The position of P1 at the top of the slope reduces the chances of infiltration. However, the pore water pressure of P1 is among the highest. Therefore, the value of FOS for P1 remains stable. The increase in pore water pressure diminished the grain-to-grain friction effect at P4 and caused landslides.

FOS inspired the DL design, but the most distinct aspect is that the hazard range was more specifically categorized. Because the risk factor values increased to 1, the hazard level value did not go beyond 1. The use of AHP provides each category's rank and priority. The rank is based on nine criteria of the AHP scale introduced by Goepel (2019), as shown in Table 8.

Table 8. AHP scale criteria (Goepel, 2019).

Scale	Criteria
1	equal importance
2	weak or slight
3	moderate importance
4	moderate plus
5	strong importance
6	strong plus
7	very strong importance
8	very, very strong
9	extreme importance

While the significance of each category is emphasized, priority and rank are required for the combined categories to regulate the level of hazard. The top priority categories are FOS with 43.0%, followed by rainfall with 32.8%, OSHA soil classification 15.7%, and soil-water infiltration with 8.5%. The FOS is of the highest rank because steep and unstable slopes can slide without triggering factors such as precipitation and a high infiltration rate. Rainfall is ranked second, as heavy and prolonged precipitation places stable slopes at risk. A stable slope can be affected by this kind of rainfall, which would lead to an unsteady slope where the mass of earth will start sliding. The OSHA soil classification places on the bottom level. Type A stable soil can be classified as type C if the soil has been altered for road construction, bridges, or tunnels. Therefore, the priority percentages and levels are low. When comparing the criteria, soil infiltration on flat terrain is given a lower priority because it has no slope and does not cause any change in the soil. This indicates that penetration depends on top priorities such as FOS, heavy rainfall and soil classification.

The parameter is separated into each factor by dividing the priority percentage from the lowest to the highest level of impact (Table 9) after obtaining the priority percentage and rank acquisition. In precipitation and FOS, the highest risk for potential landslide categories is 0. The other risk value is determined for the unlikely risk of landslides, as there are only two categories. The danger score contrasts with the probability score. More than two categories require the initial score set with the lowest risk score and increases until it reaches the maximum risk score. The high impact level indicates a high probability of landslides.

Table 9. Danger level.

	Value	Probability of Landslide	Impact	Risk Score	Danger Value	Danger Score
		Rain				
Landslide	0	High	2	32.8	0	0
No landslide	1	Low	1		32.8	0.328
		FOS				
Unstable	<1	High	2	43.0	0	0
Stable	>1	Low	1		43.0	0.43
		Soil type OSHA				
Type C (unstable)	gravel sand loamy sand submerged soil soil with water freely seeping submerge rock that is not stable	High	3	15.7	5.233	0.052

Type B (moderate)	angular gravel silt silty loam sandy loam silty clay loam sandy clay loam	medium	2		10.466	0.105
Type A (stable)	clay silty clay sandy clay clay loam silty clay loam sandy clay loam	Low	1		15.7	0.157

Soil Study Area						
Point 3	Silty gravel	Very high	4	8.5	2.125	0.021
Point 4	Silty gravel	High	3		4.25	0.043
Point 2	Silty gravel	Moderate	2		6.375	0.064
Point 1	Sandy silt	Low	1		8.5	0.085
				TOTAL	**100**	**1**

Four main frameworks are used as a basis to design the DL by producing value elements that represent landslide hazards. DL is arranged into low, moderate, high, and very high slope risks that range between (0.76–1), (0.51–0.75), (0.26–0.50) and (0–0.25), respectively. This classification serves as an indicator for regulating the level of slope safety. The DL value for P1 to P4 is shown in Table 10.

Table 10. Danger level result of the slope.

	R DS	F DS	O DS	S DS	DL	Slope risk
Point 1	0	0.43	0.052	0.085	0.567	Moderate
Point 2	0	0	0.052	0.064	0.116	Very high
Point 3	0	0	0.052	0.021	0.073	Very high
Point 4	0	0	0.052	0.043	0.095	Very high

The results indicate that the slope of the study area poses a very high risk of landslides. Three out of four DL monitoring points are below 0.25, indicating a high-risk slope. Only the highest monitoring point, P1, has a moderate slope risk, but due to a weak lower slope, P1 is also exposed to slope failure.

Conclusions

The newly developed DL approach introduces the integration of rainfall, infiltration, FOS and soil classification. Each parameter has a significant impact on the estimation and prediction of landslides. From a practical point of view, the advantage of the proposed method is in predicting the variability of saturated slope instability along with rainfall data. Moreover, the presented DL estimate can be adapted to different soil-water patterns, soil types, surface slopes and soil characteristics. DL can also help estimate the slope stability with a clear classified range representing slope risk. The adoption of a mathematical calculation based on physical phenomena enables the acquisition of the slope strength limit, rainfall threshold and soil-water infiltration patterns that affect the slope stability. The mathematical computation carried out to measure the safety factor allowed different preliminary simulations to be carried out. The implementation is associated with an equation representing geotechnical instability conditions.

References

Alexandra, W., Barbara, T., Ning, L., Aziz, K., & Jonathan W. G. (2019). Hydrological Behavior of an Infiltration-Induced Landslide in Colorado, USA. *Geofluids*, 2019, 213-222.

Biondi, G., Cascone, E., Magueri, M., & Motta, E. (2000). Seismic response of saturated cohesionless slopes. *Soil Dynamics and Earthquake Engineering*, *20*(1–4), 209-215.

Borges, R. G., Lima, A. C., & Kowsmann, R. O. (2015). Areas susceptible to landsliding on the continental slope. In: Kowsmann, R.O., editor. *Geology and Geomorphology*. Rio de Janeiro: Elsevier. *Habitats*, 1, 99-136.

Borja, R. I., & White, J. A. (2010). Continuum deformation and stability analyses of a steep hillside slope under rainfall infiltration. *Acta Geotechnica*, *5*(1), 1–14.

Casagli, N., Dapporto, S., Ibsen, M., Tofani, V., & Vannocci, P. (2005). Analysis of the landslide triggering mechanism during the storm of 20th–21st November 2000, in Northern Tuscany. *Landslides*, *3*(1), 13–21.

Chikalamo, E. E., Mavrouli, O. C., Ettema, J., van Westen, C. J., Muntohar, A. S., & Mustofa, A. (2020). Satellite-derived rainfall thresholds for landslide early warning in Bogowonto Catchment, Central Java, Indonesia. *International Journal of Applied Earth Observation and Geoinformation*, *89*, 102093. https://doi.org/10.1016/j.jag.2020.102093.

Chow, V. T., Maidment, D. R., & Mays, L. W. (1988). *Applied Hydrology*. New York, McGraw-Hill.

Cruden, D. M., & Varnes, D. J. (1996). Landslide types and processes. In: Turner A. K.; Shuster R.L. (eds) Landslides: Investigation and Mitigation. Transportation Research Board, 1996, *Special Report* 247, 36–75.

Downer, C. W., Ogden, F. L., Neidzialek, J., & Liu, S. (2005). GSSHA: A model for simulating diverse streamflow generating processes. In V. P. Singh and D. Frevert (eds.). *Watershed models*, CRC Press.

Fabrizio de Luiz, R. L., Maria, C. V. G., & Fabiana, S. F. (2020). Evaluation of shallow landslide susceptibility and Factor of Safety variation using the TRIGRS model, Serra do Mar Mountain Range, Brazil, *Journal of South American Earth Sciences*, 107, 103011.

Gariano, S. L., & Guzzetti, F. (2016). Landslides in a changing climate. *Earth-Science Reviews* 162, 227-252.

Glade, T., Crozier, M., & Smith, P., (2000). Applying Probability Determination to Refine Landslide-triggering Rainfall Thresholds Using an Empirical "Antecedent Daily Rainfall Model". *Pure Applied Geophysics*, *157*(6–8), 1059–1079.

Green, W. H., & Ampt, G. A. (1911). Studies on soil physics: Part I. The flow of air and water through soils. *Journal of Agricultural Science*, *1911*(4), 1–24.

Griffiths, D. V., Huang, J., & Fenton, G. A. (2011). Probabilistic infinite slope analysis. *Computers and Geotechnics*, *38*(4), 577–584.

Goepel, K. D. (2019). Comparison of Judgment Scales of the Analytical Hierarchy Process-A New Approach. *International Journal of Information Technology & Decision Making*, *18*(2), 445-463.

Guo, Z., Chen, L., Gui, L., Du, J., Yin, K., & Do, H. (2020). Landslide displacement prediction based on variational mode decomposition and WA-GWO-BP model. *Landslides*, 17, 567-583.

Gutiérrez-Martín, A. (2020). A GIS-physically-based emergency methodology for predicting rainfall-induced shallow landslide zonation. *Geomorphology*, 359,

107121.

Hansen, A. (1984) Landslide hazard analysis, In: Slope Instability, (Eds.) Brunsden, D. and Prior, D. B., *John Wiley and Sons, New York*, 523–602.

Haque, U., da Silva, P. F., Devoli, G., Pilz, J., Zhao, B., Khaloua, A., Wilopo, W., Andersen, P., Lu, P., Lee, J., Yamamoto, T., Keeling, D., Wu, J., & Glass, G. E. (2019). The human cost of global warming: Deadly landslides and their triggers (1995–2014). *Science of The Total Environment*, 682, 673-684.

Hidalgo, C., & Vega, J. (2014). Hazard estimation for landslides triggered by earthquakes and rainfall (Valle de Aburrá-Colombia). *Revista EIA*, *11*(22), 103-117.

Hughes, D. A. (1998) Antecedent precipitation. In: Encyclopedia of Hydrology and Lakes. *Encyclopedia of Earth Science*. Springer, Dordrecht.

Ivanov, V., Arosio, D., Tresoldi, G., Hojat, A., Zanzi, L., Papini, M., & Longoni, L. (2020). Investigation on the Role of Water for the Stability of Shallow Landslides-Insights from Experimental Tests. *Water*, 12, 1203.

Kang, S., Cho, S., Kim, B., & Go, G. (2020). Effects of Two-Phase Flow of Water and Air on Shallow Slope Failures Induced by Rainfall: Insights from Slope Stability Assessment at a Regional Scale. *Water* 12, 812.

Khalaj, S., Bahootoroody, F., Abaei, M., Bahootoroody, A., De Carlo, F., & Abbassi, R. (2020). A methodology for uncertainty analysis of landslides triggered by an earthquake. *Computers and Geotechnics*, 117, 1-13.

Kim, J., Lee, K., Jeong, S., & Kim, G. (2014). GIS-based prediction method of landslide susceptibility using a rainfall infiltration-groundwater flow model. *Engineering Geology*, 182, 63-78.

Liu, Q. Q., & Li, J. C. (2015). Effects of Water Seepage on the Stability of Soil-slopes, *Procedia IUTAM*, 17, 29-39.

Phoon, K. K. 2008. Numerical recipes for reliability analysis - a primer. In Reliability-based design in geotechnical engineering: computations and applications. Edited by K. K. Phoon. Taylor & Francis, New York, 1–75.

Pourkhosravani, A., & Kalantari, B. (2011). A Review of Current Methods for Slope Stability Evaluation. *Electronic Journal of Geotechnical Engineering*, 16, 1245-1254.

Pradhan, S. P., & Siddique, T. (2020). Stability assessment of landslide-prone road cut rock slopes in Himalayan terrain: A finite element method-based approach, *Journal of Rock Mechanics and Geotechnical Engineering*, *12*(1), 59-73.

Rawls, W. J., Brakensiek, D. L., & Saxton, K. E. (1982). Estimation of soil-water properties. *Transactions of the ASAE*, *25*(5), 1316–1320.

Stine, M. B. (2013). Fire as a Geomorphic Agent. *Treatise on Geomorphology* 12, 236-251.

Tian, Y., Xu, C., Ma, S., Xu, X., Wang, S., & Zhang, H. (2019). Inventory and spatial distribution of landslides triggered by the 8th August 2017 MW 6.5 Jiuzhaigou earthquake, China. *Journal of Earth Science*, *30*(1), 206-217.

Travis, Q., Houston, S., Marinho, F., & Schmeeckle, M. (2009). Unsaturated Infinite Slope Stability Considering Surface Flux Conditions. *Journal of Geotechnical and Geoenvironmental Engineering*, 136, 963-974.

Tsai, T., Chen, H., & Yang, J. (2008). Numerical modelling of rainstorm-induced shallow landslides in saturated and unsaturated soils. *Environmental Geology*, *55*(6), 1269–1277.

Vahedifard, F., Mortezaei, K., Leshchinsky, B., Leshchinsky, D., & Lu, N. (2016). Role of suction stress on service state behavior of Geosynthetic-Reinforced Soil Structures. *Transportation Geotechnics*, 8, 45-56.

Van Westen, C. J., & Terlien, M. T. J. (1996). An approach to-wards deterministic landslide hazard analysis in GIS: a case study from Manizales (Colombia). *Earth Surface Processes and Landforms*, *21*(9), 853-868.

Zêzere, J. L., Trigo, R. M., & Trigo, I. F. (2005). Shallow and deep landslides induced by rainfall in the Lisbon region (Portugal): assessment of relationships with the North Atlantic Oscillation. *Natural Hazards Earth System Science*, 5, 331–344.

Zhao, B., Dai, Q., Han, D., Dai, H., Mao, J., & Zhuo, L. (2019). Antecedent wetness and rainfall information in landslide threshold definition. *Hydrology and Earth System Sciences Discussions*, 1–26. https://doi.org/10.5194/hess-2019-150.